

STRUCTURAL BIOLOGY

Critical role of spectrin in hearing development and deafness

Yan Liu^{1*}, Jieyu Qi^{1,2,3*}, Xin Chen^{4*}, Mingliang Tang^{2,3*}, Cenfeng Chu^{1,4}, Weijie Zhu^{1,2,3}, Hui Li¹, Cuiping Tian¹, Guang Yang⁵, Chao Zhong⁶, Ying Zhang⁷, Guangjian Ni^{8,9}, Shuijin He^{4†}, Renjie Chai^{2,3,10,11,12†}, Guisheng Zhong^{1,3,4,13†}

Inner ear hair cells (HCs) detect sound through the deflection of mechanosensory stereocilia. Stereocilia are inserted into the cuticular plate of HCs by parallel actin rootlets, where they convert sound-induced mechanical vibrations into electrical signals. The molecules that support these rootlets and enable them to withstand constant mechanical stresses underpin our ability to hear. However, the structures of these molecules have remained unknown. We hypothesized that α II- and β II-spectrin subunits fulfill this role, and investigated their structural organization in rodent HCs. Using super-resolution fluorescence imaging, we found that spectrin formed ring-like structures around the base of stereocilia rootlets. These spectrin rings were associated with the hearing ability of mice. Further, HC-specific, β II-spectrin knockout mice displayed profound deafness. Overall, our work has identified and characterized structures of spectrin that play a crucial role in mammalian hearing development.

INTRODUCTION

The cuticular plate of hair cells (HCs) is thought to be critical in mammalian hearing by securing stereocilia rootlets in place (1–6) and providing them with the rigidity and support necessary for auditory transduction (6–9). Stereocilia rootlets are electron-dense structures penetrating into the cuticular plate and forming an anchoring complex. This anchoring complex is believed to be the key structural component for stereocilia to withstand constant mechanical stresses, and thus plays a critical role in hearing (10). However, the specific anchoring molecules that provide stereocilia rootlets with their necessary elasticity and flexibility remain elusive.

We hypothesized that spectrin is a likely candidate to fulfill this role. Spectrin is expressed in almost all cells (11), playing a variety of important roles (11–14). In particular, the spectrin α and β subunits form flexible fiber-like structures in many types of cells (11, 14, 15). They are assembled into antiparallel heterodimers, which, in turn, form end-to-end tetramers (11, 15). Recent studies have shown that spectrin can form different structural organizations in many types of cells, although the components are similar (16–18). It is known that spectrin isoforms are expressed in dif-

ferent regions of the inner ear HCs and that they are concentrated in the cuticular plate (19, 20). However, the spectrin ultrastructural organization and therefore its role in mammalian hearing are unclear.

RESULTS

Spectrin forms ring structures in the cuticular plate

To determine the extent to which spectrin structures underpin the function of stereocilia, we turned to super-resolution fluorescence imaging, which can provide molecular labeling specificity and live-cell imaging feasibility with nanoscale resolution (21–24). Immunostaining experiments investigated the structure of both α II- and β II-spectrin in the cuticular plates of HCs of mice (fig. S1A). Confocal imaging showed the enrichment of both α II- and β II-spectrin as individual dots in the cuticular plate, but no obvious organizational pattern was detected (fig. S1B). Conversely, stimulated emission depletion (STED) imaging revealed a remarkably regular organization, with both α II- and β II-spectrin forming two rows of ring-like structures with diameters ranging from 200 to 210 nm outlining the edges of the outer HC (OHC) and inner HC (IHC) stereocilia rootlets (Fig. 1A). α II- and β II-spectrin ring structures were observed in the apex, middle, and base regions of the cochlea, and their diameters were similar (fig. S1, C and D).

To investigate the spatial relation between individual spectrin rings and rootlets, we performed two-color STED imaging to characterize the structure of spectrin and F-actin bundles in the cuticular plate, which forms the central part of rootlets and was labeled with phalloidin-conjugated organic dyes. The STED results showed that each spectrin ring surrounded an F-actin dot (Fig. 1B), supporting the idea that the spectrin rings associate tightly with rootlets in the cuticular plate. Transmission electron microscopy of cochlear sections from mice found a mean stereocilia rootlet diameter of ~80 nm, which is comparable to previous findings (5, 6) but smaller than the mean diameter of the rings of spectrin (Fig. 1, C and D). We reasoned that spectrin forms cylinders that wrap around the rootlets acting as a mechanical sensor during stereocilium deflection because of its intrinsic extensibility and elasticity (25, 26). Given the highly conserved organization of spectrin

Copyright © 2019 The Authors, some rights reserved; exclusive licensee American Association for the Advancement of Science. No claim to original U.S. Government Works. Distributed under a Creative Commons Attribution NonCommercial License 4.0 (CC BY-NC).

¹Human Institute, ShanghaiTech University, Shanghai, China. ²Key Laboratory for Developmental Genes and Human Disease, Ministry of Education, Institute of Life Sciences, Jiangsu Province High-Tech Key Laboratory for Bio-Medical Research, Southeast University, Nanjing, China. ³Co-innovation Center of Neuroregeneration, Jiangsu Key Laboratory of Neuroregeneration, Nantong University, Nantong, China. ⁴School of Life Science and Technology, ShanghaiTech University, Shanghai, China. ⁵Shanghai Institute for Advanced Immunochemical Studies, ShanghaiTech University, Shanghai, China. ⁶School of Physical Science and Technology, ShanghaiTech University, Shanghai, China. ⁷Department of Medical Neuroscience, Faculty of Medicine, Dalhousie University, 5850 College Street, Halifax, Canada. ⁸Academy of Medical Engineering and Translational Medicine, Tianjin University, Tianjin, China. ⁹Laboratory of Neural Engineering and Rehabilitation, Department of Biomedical Engineering, College of Precision Instruments and Optoelectronics Engineering, Tianjin University, Tianjin, China. ¹⁰Institute for Stem Cell and Regeneration, Chinese Academy of Sciences, Beijing, China. ¹¹Research Institute of Otolaryngology, No.321 Zhongshan Road, Nanjing, China. ¹²Beijing Key Laboratory of Neural Regeneration and Repair, Capital Medical University, Beijing, 100069, China. ¹³Guangzhou Institute of Biomedicine and Health, Chinese Academy of Sciences, Guangzhou, China.

*These authors contributed equally to this work.

†Corresponding author. Email: heshj@shanghaitech.edu.cn (S.H.); renjie@seu.edu.cn (R.C.); zhongsh@shanghaitech.edu.cn (G.Z.)

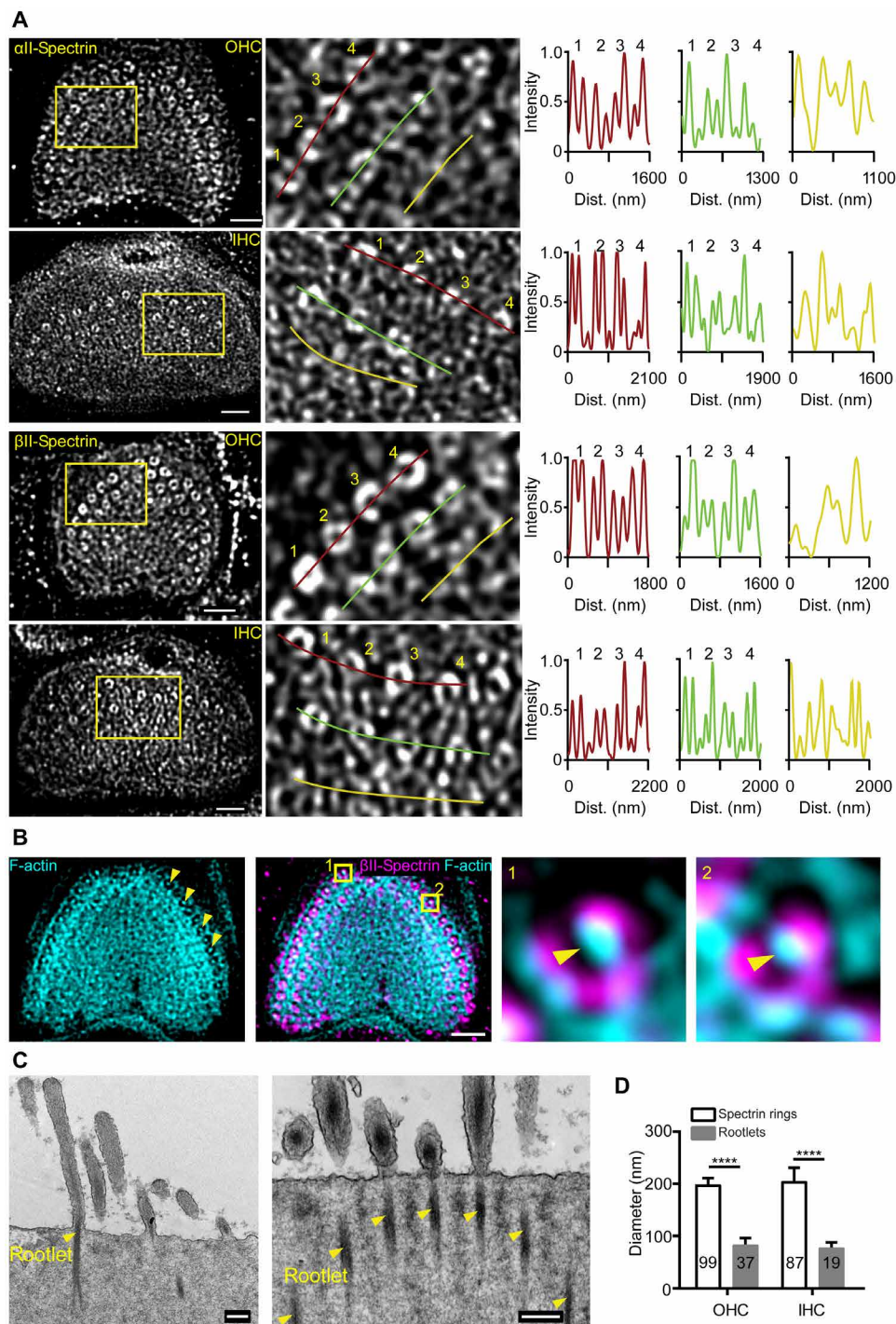


Fig. 1. Structure of α II- and β II-spectrin in the cuticular plate. (A) Representative STED images of α II- and β II-spectrin from mouse OHCs and IHCs at P21, with magnification of yellow boxed regions on the right. Intensity profiles along the solid lines are shown. The rings are numerically labeled, and corresponding intensity curves are shown ($n = 3$ mice). Scale bars, 1 μ m. (B) Representative two-color STED image of β II-spectrin (magenta) and F-actin (cyan) in the cuticular plate of OHC and the magnification region indicated by yellow boxes. Yellow triangles indicate that the rootlet is found inside the spectrin ring. Scale bar, 1 μ m. (C) Representative transmission electron micrographs of the apical region of HCs from mice, with the sections parallel to the stereocilia staircase (left) and stereocilia row (right) ($n = 3$ mice). Scale bars, 200 nm. (D) Size comparison among spectrin rings and stereocilia rootlets. $n =$ ring numbers or rootlet numbers from three to five mice for each group. **** $P < 0.0001$, Student's t test. Error bars \pm SD.

molecules (27), our results suggest that α II- and β II-spectrin form flexible tetramers outlining the edges of the stereocilia rootlets of OHCs and IHCs in the cuticular plate.

Three-dimensional STED images showed that the rings were aligned at different depths extending more than 600 nm into the cuticular plate (fig. S1, E and F). The diameter of the rings did not change along the different layers of the stereocilia axis. The aligned spatial pattern of spectrin rings in three dimensions may strengthen their stiffness and flexibility to hold stereocilia in place after deflections. Spectrin displayed ring-like structures with similar diameter in the HCs of different species of bats or rats, indicating the functional importance of these spectrin rings. Thus, we propose that α II- and β II-spectrin form heterotetramers and cylindrical structures that wrap around the circumference of stereocilia rootlets, likely providing the requisite mechanical support and elasticity.

Notably, we observed two rows of spectrin rings in the cuticular plate that hold three rows of stereocilia (Fig. 1A; fig. S1, C and D; and movie S1). The third row of stereocilia is thinner and lower than the top two rows. We hypothesized that spectrin rings may be required for the function of larger stereocilia. To test our hypothesis, we made two sets of observations: imaging the spectrin ring formation during development in OHCs and IHCs and imaging spectrin structure in vestibular HCs (VHCs) where the villi are thinner. Spectrin rings were not formed, although stereocilia were visible in both OHCs and IHCs during the early development (Fig. 2, A to D), suggesting that spectrin rings are not required for the formation of stereocilia. Spectrin rings are formed starting from 2 weeks after birth when stereocilia are thicker than those at early developmental stages (Fig. 2, A to D), implying that spectrin rings may be associated with the maintenance of stereocilia and functioning of HCs. The diameter of spectrin was not different in OHCs and IHCs at different developmental stages (Fig. 2E). Further, in VHCs, spectrin was distributed in a meshwork arrangement in the cuticular plate region, but no rings were observed (Fig. 2, F and G; and movie S2). Thus, our results support the idea that spectrin rings are not required for the formation of stereocilia but may be strongly associated with the functioning of the thicker stereocilia of OHCs and IHCs.

β II-Spectrin is essential for the polarity and function of HCs and hearing development

To directly analyze the effects of spectrin on hearing function, we crossed *Sptbn1-flox* (*Sptbn1^{flox/flox}*) mice with *Atoh1^{cre/+}* mice, which express a Cre recombinase in the HC-specific *Atoh1* locus to generate HC-specific β II-spectrin knockout (*Atoh1-Sptbn1^{-/-}*) mice (Fig. 3A). We performed immunostaining experiments to characterize the β II-spectrin expression in the apical, middle, and base regions of cuticular plate in *Atoh1-Sptbn1^{-/-}* mice. β II-spectrin was completely deleted in all regions of cuticular plate in *Atoh1-Sptbn1^{-/-}* mice (Fig. 3B). Because α II-spectrin exists in cuticular plate of HCs and may play a complementary role for β II-spectrin in HCs, we tested whether the expression of α II-spectrin was altered in *Atoh1-Sptbn1^{-/-}* mice. Our immunostaining experiments indicated a near-complete deletion of α II-spectrin in cuticular plates and the fonticulus region of HCs in *Atoh1-Sptbn1^{-/-}* mice at 2 weeks after birth (Fig. 3C). α II-spectrin was previously found in the cortical lattice, which is likely associated with β V-spectrin in HCs (19). Notably, α II-spectrin was found specifically in the cortical lattice region of HCs in *Atoh1-Sptbn1^{-/-}* mice (Fig. 3C), suggesting that β II-spectrin may be required for the specific location of α II-spectrin in the cuticular

plate of HCs. Next, we tested whether β II-spectrin affects the distribution of other proteins in the taper region of stereocilia. We immunostained taperin in HCs from *Atoh1-Sptbn1^{-/-}* mice. The amount of taperin expression was quite normal, but its spatial pattern was markedly changed according to the spatial pattern of stereocilia (Fig. 3D). Looking into details, taperin was located in the taper region of each stereocilium and also outside the taper region of stereocilia (Fig. 3D). FAM65B was found to be expressed in the base region of stereocilia and critical for hearing development (28). FAM65B expression level was not substantially decreased, but FAM65B spatial pattern was substantially changed in HCs of *Atoh1-Sptbn1^{-/-}* mice (fig. S2). Our results suggested that β II-spectrin is important for the normal distribution of taperin and FAM65B in the base region of stereocilia.

Next, we imaged the F-actin structure at different stages of HC development in *Atoh1-sptbn1^{-/-}* mice. Typically, OHCs displayed a V-shape organization of stereocilia even at early development, which can be detected by the F-actin structure of HCs (Fig. 4A). The stereocilia started to lose their polarity and developed dysregulated spacing as early as postnatal day 4 (P4) in *Atoh1-sptbn1^{-/-}* mice (Fig. 4B). The extent of the disruption was larger at later developmental stages (Fig. 4, A and B). Further, we characterized the HC morphology by immunostaining myosin7a and found that HCs were gradually degraded during development in *Atoh1-sptbn1^{-/-}* mice (fig. S3). HCs started to degenerate at around 2 weeks after birth, and this supports the idea that spectrin in the HC is essential to HC development and that it might affect its polarity and the disruption of protein distribution, specifically in the cuticular plate region (fig. S3). We further examined the expression of spectrin and F-actin in VHCs in the *Atoh1-sptbn1^{-/-}* mice. β II-spectrin was completely deleted in VHCs of *Atoh1-sptbn1^{-/-}* mice (fig. S4A). The morphology of VHCs was assessed by fluorescence-labeled phalloidin, and no obvious defects were visualized in VHCs of *Atoh1-sptbn1^{-/-}* mice (fig. S4B). Notably, no circling or head tilt behaviors were observed from *Atoh1-sptbn1^{-/-}* mice. Furthermore, vestibular ocular reflex (VOR) has been measured for assessment of vestibular function, and no significant difference was observed between *Atoh1-sptbn1^{-/-}* mice and control mice (fig. S4C). These results suggest that β II-spectrin deletion did not substantially affect the function of VHCs. Next, to study the role of β II-spectrin in HCs in hearing development, we performed auditory brainstem response (ABR) tests to assess the hearing ability of *Atoh1-Sptbn1^{-/-}* mice. We found that the *Atoh1-Sptbn1^{-/-}* mice displayed severe hearing loss (Fig. 4, C and D). Our results demonstrate a crucial role of spectrin in HC function and hearing development.

Spectrin rings correlate with hearing ability

Mice acquire the ability to hear at around 2 weeks after birth (29), which corresponds to our observation of spectrin forming organized structures in the cuticular plate and playing an essential role in hearing development. Additionally, we wished to investigate whether spectrin is necessary for the maintenance of hearing in adults. As follows, we investigated the structure of spectrin rings in mice with hearing disability due to aging or noise exposure. We hypothesized that spectrin's regular ring-like organization would be perturbed under both HC damage conditions.

In aging mice, hearing function was gradually lost over time (Fig. 5A), as measured by ABR tests. β II-spectrin rings were also gradually disrupted in the OHCs of aging mice (Fig. 5B) and were

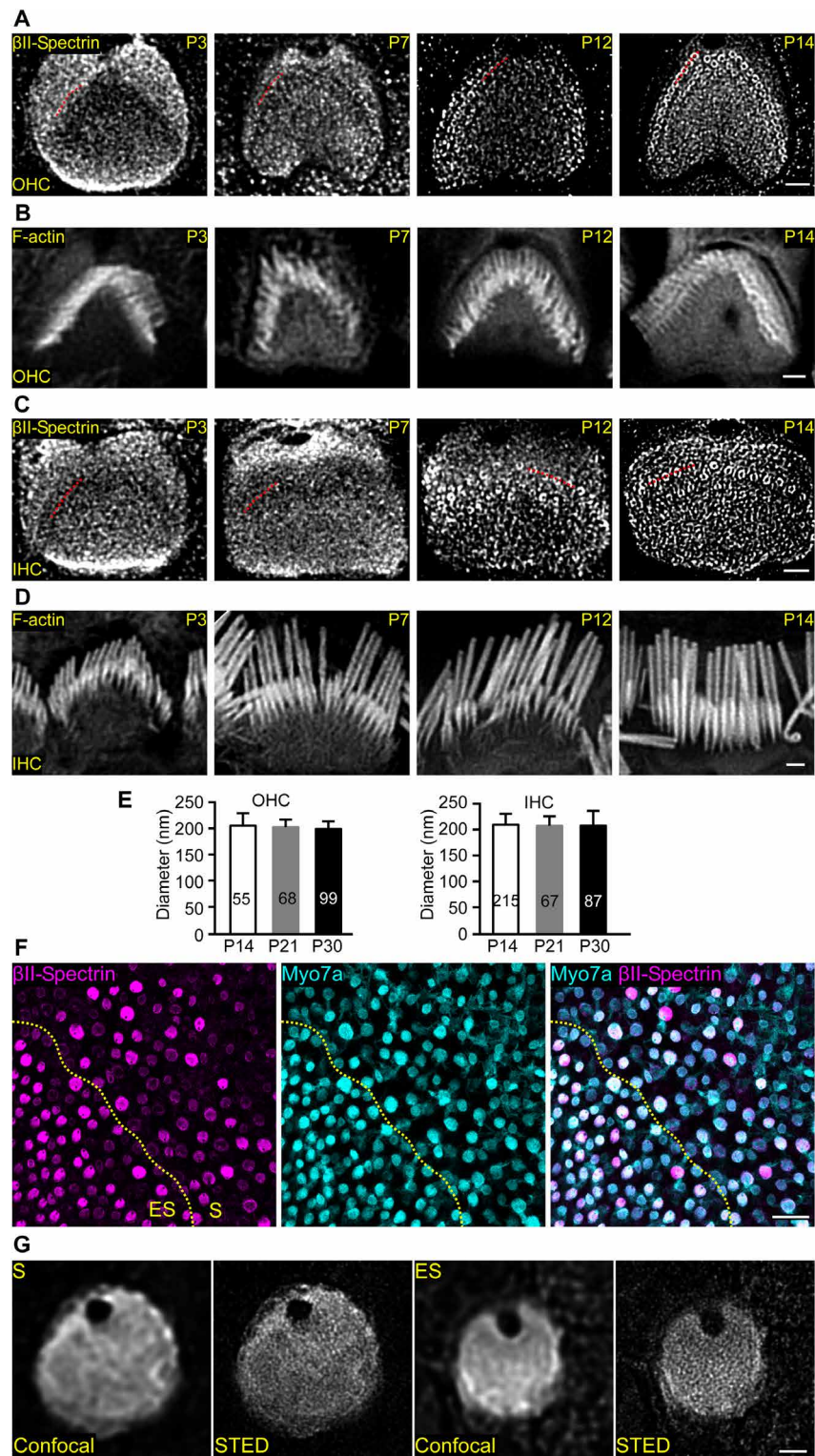


Fig. 2. Spectrin structure in HCs during postnatal development. (A) Representative STED images of β II-spectrin staining in the cuticular plates of OHCs at different developmental stages. $n = 3$ to 8 mice from each stage. Scale bar, 1 μ m. (B) Representative confocal images of stereocilia in OHCs at different developmental stages ($n = 3$ to 5 mice from each stage). Scale bar, 1 μ m. (C and D) Same as (A) and (B), but for IHCs at different developmental stages. (C) $n = 4$ to 9 mice from each stage; (D) $n = 3$ to 5 mice from each stage. Scale bars, 1 μ m. (E) Spectrin ring diameter comparison among different developmental stages in OHCs and IHCs, respectively. $n =$ ring numbers from three to five mice for each group. No significances. Two-way analysis of variance (ANOVA). Error bars \pm SD. (F) Representative confocal images of β II-spectrin (magenta) and myosin7a (cyan) in utricle from P14 mice ($n = 3$ mice). S, striolar region; ES, extrastriolar region. Scale bar, 15 μ m. (G) Representative confocal and STED images of β II-spectrin in VHCs ($n = 3$ mice). Scale bar, 1 μ m.

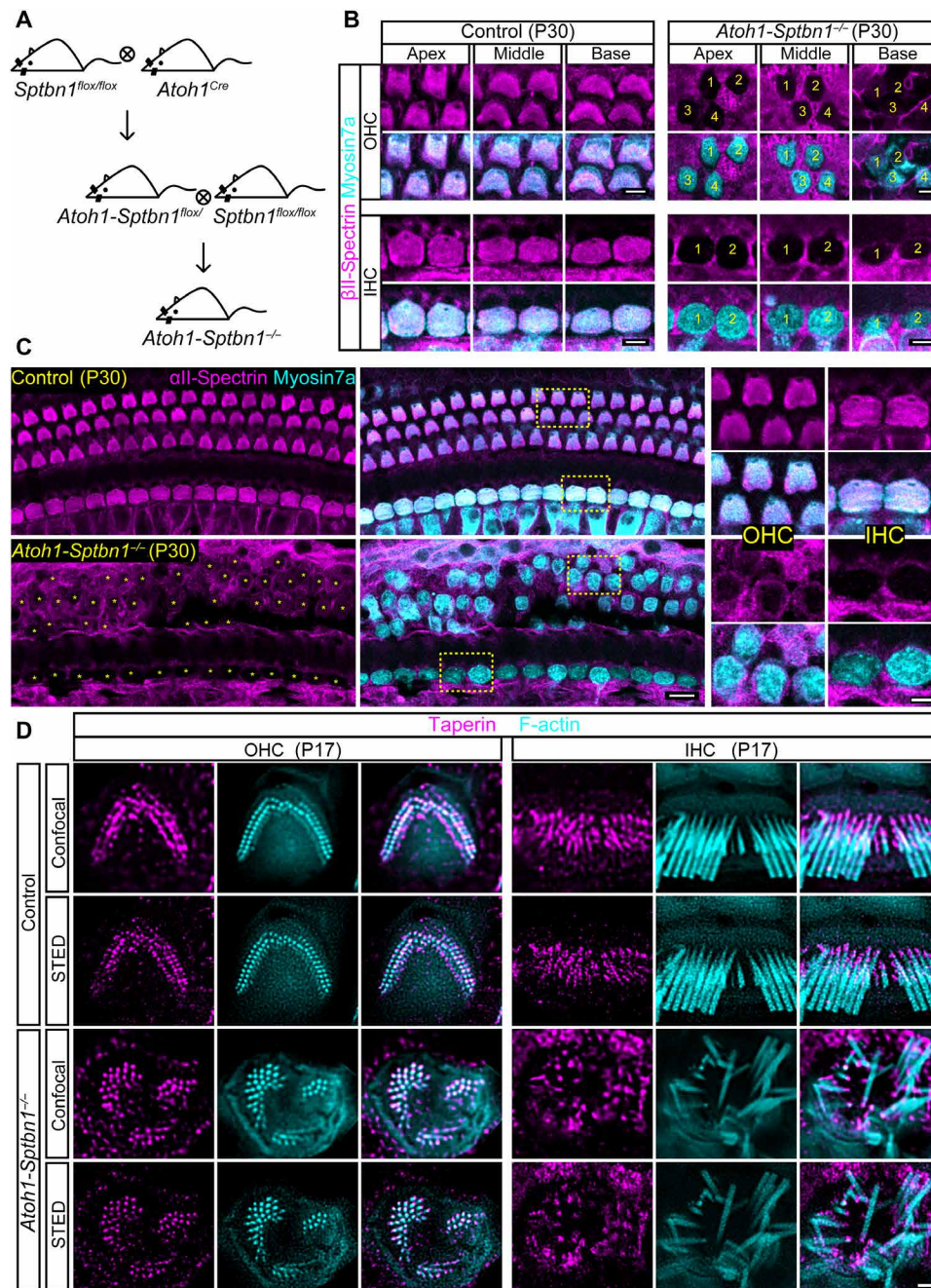


Fig. 3. Spectrin is required for the right distribution of taperin in HCs. (A) Schematic methodology of generating β II-spectrin HC-specific KO mice. (B) Representative confocal images of β II-spectrin signals in the HCs in apical, middle, and basal turns from control mice ($n = 3$ mice) and *Atoh1-Sptbn1^{-/-}* mice at P30 ($n = 3$ mice). Yellow numbers indicate the location of HCs. Scale bars, 4 μ m. (C) Same as (B), but for *all*-spectrin ($n = 3$ mice). Scale bars, 10 μ m (left) and 5 μ m (right). (D) Representative confocal and STED images of taperin (magenta) and F-actin (cyan) from control mice ($n = 3$ mice) and *Atoh1-Sptbn1^{-/-}* mice ($n = 3$ mice) at P17. Scale bar, 1 μ m.

more disrupted in the base region of their OHCs in line with the degree of hearing loss at high frequencies (Fig. 5C). In the noise-induced permanent threshold shift (PTS) mouse model, we tested the structure of β II-spectrin rings (fig. S4A). Notably, we examined the spectrin structure 1 day after noise exposure and observed that spectrin rings were severely disrupted in the cuticular plate of OHCs in these mice (fig. S4, A to C). Our results indicate that the nanoscale structure of some proteins in these seemingly normal

HCs was already disrupted and that the level of disruption of spectrin rings correlates with the degree of hearing disability in both aging and PTS mice. Further, we used a finite element model of the organ of Corti to test whether the spectrin rings play a role in the cochlear amplifier (30). Micromechanics modeling showed that the loss of spectrin rings had a direct depressive effect on the basilar membrane (BM) displacement amplitude (Fig. 5D) and thus played a crucial role in hearing. Without spectrin rings, the modeling result

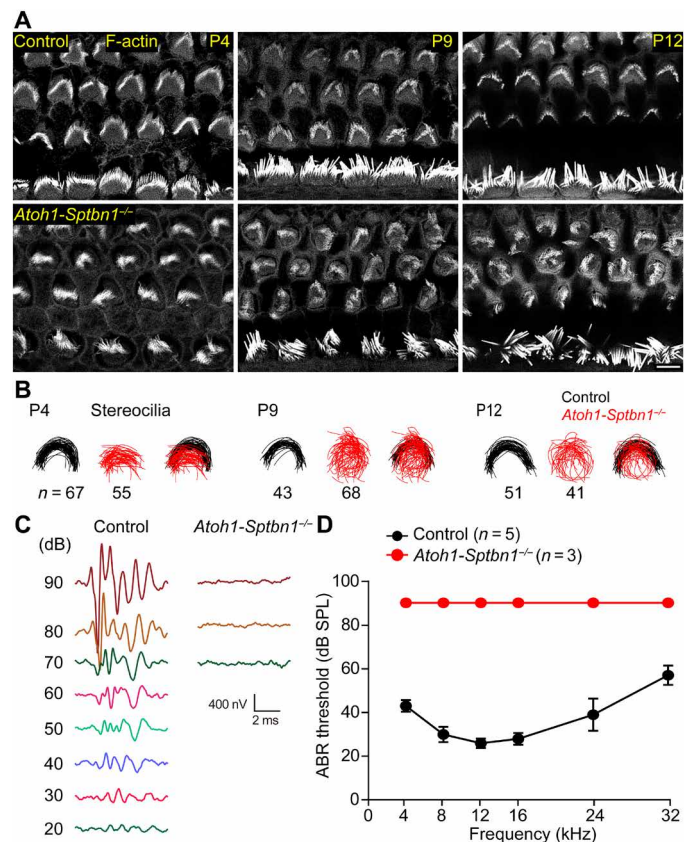


Fig. 4. Spectrin is essential for HCs and hearing development. (A) Representative confocal images of F-actin from control mice and *Atoh1-Sptbn1*^{-/-} mice at P4 (*n* = 3 mice), P9 (*n* = 3 mice), and P12 (*n* = 3 mice). Scale bar, 5 μ m. (B) Stereocilia morphology tracing in the cuticular plate of OHCs from control mice and *Atoh1-Sptbn1*^{-/-} mice at P4, P9, and P12. The root of stereocilia from each HC was traced to determine the polarity changes of stereocilia. We first aligned the edges of each OHC to ensure that the relative position of the stereocilia is comparable to each other, and then we drew a line along the roots of the stereocilia to show the changes of stereocilia polarity. *n* = tracing numbers from three to five mice for each group. (C) Representative ABR traces recorded from control mice (*n* = 5 mice) and *Atoh1-Sptbn1*^{-/-} mice (*n* = 3 mice) at P30, with a 12-kHz tone burst between 20 and 90 dB. (D) ABR results of control and *Atoh1-Sptbn1*^{-/-} mice. Error bars \pm SD.

indicated a severe effect on the displacement amplitude of BM (Fig. 5D). Thus, we hypothesized that mice without spectrin rings display severe hearing loss or even deafness.

DISCUSSION

Together, using super-resolution fluorescence microscope, we have identified a previously unknown structure of spectrin in the cuticular plate of HCs: α II- and β II-spectrin form a cylindrical structure corresponding to each stereocilium in the rootlet region. Furthermore, we have provided evidence that spectrin in HCs plays a critical role in hearing development and deafness.

Spectrin as a mechanical support for rootlets and shear mechanical stress

Our previous studies support the idea that spectrin tends to form a periodic structure under the plasma membrane in a concentration-dependent manner in either neurons or glial cells (17, 27). Spectrin

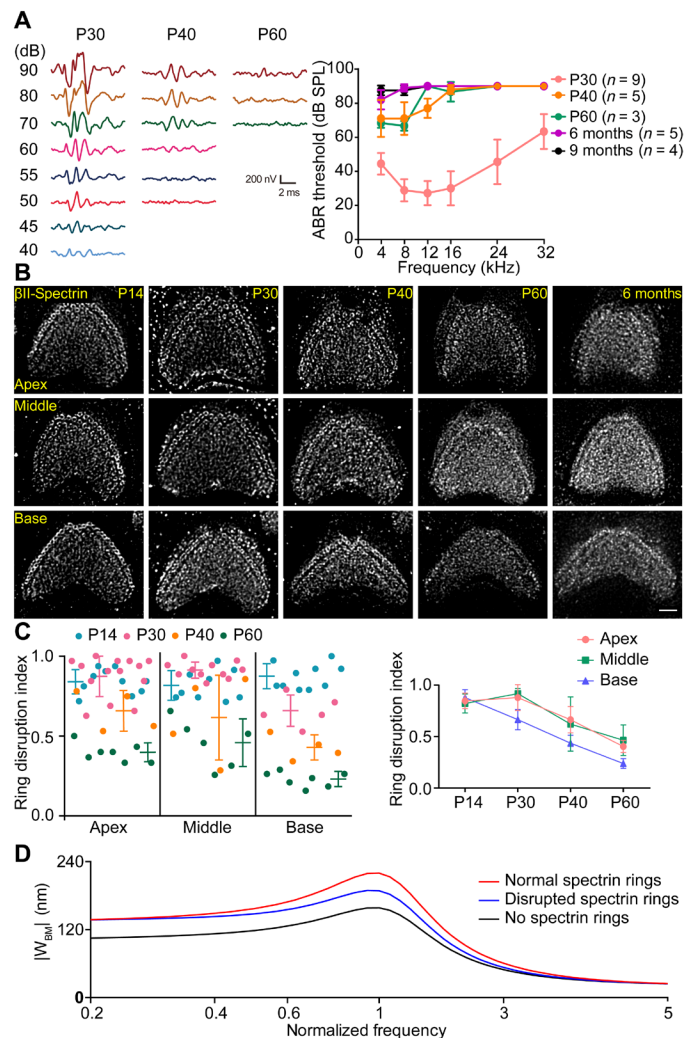


Fig. 5. Spectrin rings are associated with hearing ability. (A) Left: Representative traces recorded from CD-1 mice at P30, P40, and P60. The stimulus was a 12-kHz tone burst between 40 and 90 dB. Right: Representative ABR results of CD-1 mice at P30, P40, P60, 6 months, and 9 months. *n* = mice numbers from different developmental stages. (B) Representative STED images of β II-spectrin in the apical, middle, and basal turns from P14, P30, P40, P60, and 6-month CD-1 mice. *n* = 3 mice from each stage. Scale bar, 1 μ m. (C) Ring disruption index of P14 (*n* = 29 cells from five mice), P30 (*n* = 30 cells from four mice), P40 (*n* = 16 cells from three mice), and P60 (*n* = 20 cells from three mice) CD-1 mice. (D) The predicted transverse motions of BM were compared under different conditions: normal spectrin rings, reduced spectrin rings, and no spectrin rings in the cuticular plate of the OHCs. Normalized frequency was calculated as $\text{Freq}/\text{CF}(\times 0)$. $|W_{\text{BM}}|$, BM displacement. Error bars \pm SD.

concentrates in the rootlet region of HCs, which could be self-assembled into higher-order structures like those found in neurons or glial cells. Spectrin likely forms heterotetramers, which, in turn, form cylindrical structures perpendicular to the cellular submembrane cortex, and this organization is in marked contrast to those structures in neurons or red blood cells (17, 18, 27). These intracellular spectrin structures corresponding to each stereocilium may help to maintain its function because of the intrinsic extensibility and flexibility of spectrin. The cylindrical spectrin structure may help rootlets shear mechanical stress during deflection. Previous studies have supported an elastic function for spectrin (14). β -Spectrin is

required for membrane elasticity, which is essential for red blood cells to withstand deformation when passing through arterioles (26). Neurons can be stretched up to 65% of their length without breaking, and spectrin has been proposed to be involved in maintaining membrane elasticity (31). Thus, spectrin forms an isolated and specific nanodomain in the cuticular plate corresponding to each rootlet, helping to maintain stereocilium function.

Spectrin as an intracellular trafficking protein

We propose that this cylindrical structure perpendicular to the cell membrane maintains stereocilia by allowing molecules into and out of the stereocilium. Some inherited neuronal diseases are the direct result of mutations in β -spectrin (32) such as an inherited progressive spinocerebellar ataxia (SCA5) (33, 34). Mutations in β III-spectrin are related to the dislocation of membrane proteins (33); this association suggests that spectrin could act as a trafficking protein for each stereocilium and thus could be involved in developing and maintaining stereocilium identity and function.

Spectrin is critical to HC polarity and survival

In early developmental stages, HC polarity is disrupted in the absence of β II-spectrin, and the extent of the disruption becomes largest in later developmental stages such that eventually the HC starts to degenerate around 2 weeks after birth. Our data suggest that β II-spectrin is required for the normal expression pattern of proteins, such as α II-spectrin and FAM65B. In the cuticular plate, it is likely that spectrin and other components form a functional domain, which is required for HC polarity and function. The spectrin rings are formed during the maturation of membrane properties of HCs, likely by dictating the trafficking of molecules into and out of the stereocilium. Further, spectrin rings were associated with hearing ability in different animal models of hearing loss, supporting the idea that spectrin rings may be required for maturation of stereocilia and HCs. These results support a crucial role of spectrin in the cuticular plate for hearing development. Our study with multiple approaches provides a structural basis for understanding the function of spectrin in the auditory system.

MATERIALS AND METHODS

Experimental design

The objective of this study was to analyze the subdiffraction-limited structure of spectrin in HCs, followed by functional investigations of spectrin in HCs with regard to hearing ability. STED microscopy improves the resolution of imaging system up to nanometer level. Thus, the fine spectrin structure in HCs was revealed using this technology. The phenotype in spectrin-specific knockout mice with hearing disability demonstrated the critical role of spectrin in HC and proper hearing function.

Animals

C57BL/6 mice, CD-1 mice, Sprague-Dawley rats, *Sptbn1*^{flox/flox} (Jax mice, stock no. 020288), and *Atoh1-Cre* (35) mice of both sexes were used in this study. *Sptbn1*^{flox/flox} mice were mated with *Atoh1-cre* mice to spatially eliminate β II-spectrin in inner ear HCs. The day of birth was counted from P0. Genotyping primers for *Sptbn1*^{flox/flox} and *Atoh1-Cre* mice were as follows: *Sptbn1*^{flox/flox}, 5'-GTAGCCTCCTTCTGGGATG-3' (forward) and 5'-TAGAGCCCCTTCCATGGTCT-3' (reverse); *Atoh1-WT*, 5'-TGACGCCACAGCCACCTGCTA-3'

(forward) and 5'-GGACAGCTTCTTGTCGTTGTTG-3' (reverse); and *Atoh1-Cre*, 5'-GCGCAGCGCCTTCAGCAAC-3' (forward) and 5'-GCCCAAATGTTGCTGGATAGT-3' (reverse). Animals were housed under a 12-hour light/dark cycle at a room temperature of 22° ± 1°C with food and water available ad libitum. All experiments were approved by the Institutional Animal Care and Use Committees of ShanghaiTech University and Southeast University, China.

Immunohistochemistry

Mice were sacrificed with an overdose of pentobarbital sodium (100 mg/kg body weight, intraperitoneally), and the temporal bone was rapidly dissected out under the stereoscope in cold phosphate-buffered saline (PBS) (pH 7.2). To obtain whole-mount preparations of the organ of Corti from mice before P7, the cochlear spiral was microdissected from the temporal bone and adhered to a microscope slide cover glass (thickness, 0.17 mm; diameter, 10 mm) coated with Cell-Tak (BD Biosciences). Cochleae were fixed for 1 hour in 4% paraformaldehyde (in PBS, pH 7.2) at room temperature. For cochleae from mice older than P7, the temporal bone was fixed in 4% paraformaldehyde (in PBS, pH 7.2) for 2 hours at room temperature before being cut into pieces after 0.5- to 6-hour treatment of 0.5 mM EDTA (pH 8.0) until the temporal bone became soft. After complete washing with 0.01 M PBS, samples were immersed in blocking solution containing 10% donkey serum, 0.3% Triton X-100, 1% bovine serum albumin, and 0.02% sodium azide (NaN₃) in PBS (pH 7.2) for 1 to 2 hours at room temperature. We used a mouse monoclonal antibody that specifically targets the C terminus of β II-spectrin (amino acids 2101 to 2189; Santa Cruz Biotechnology, catalog no. SC-136074) or a mouse monoclonal antibody that specifically targets α II-spectrin (clone D8BI7, BioLegend, catalog no. 803201) to label different isoforms of spectrin (11, 12, 17, 27). These cochlear tissues were subsequently incubated with the primary antibody at 4°C overnight. After complete washing with PBS, the samples were incubated with the secondary antibody Alexa Fluor 555-conjugated donkey anti-mouse IgG (H+L) (Thermo Fisher Scientific, catalog no. A-31570) for 1 hour at room temperature. Cochlear samples were mounted with ProLong Gold (Life Technologies) or Vectashield (Vector Labs) mounting medium. To label F-actin in whole-mount rodent cochlear preparations, phalloidin conjugated with fluorescent dyes (Alexa Fluor 488, Thermo Fisher Scientific, catalog no. A12379; ATTO 488, ATTO-TEC, catalog no. AD488-82) was used. After the staining procedures, all samples were carefully examined under a conventional confocal microscope (Zeiss LSM700), and only those samples with high specificity and preferable signal-to-noise ratio were selected for further super-resolution imaging.

STED imaging

STED images were obtained with a Leica TCS SP8 STED 3X microscope equipped with a white light pulse laser (WLL2), STED laser (592 nm), an oil immersion 100 \times /numerical aperture 1.4 objective lens (HC PL APO CS2, Leica), and a TCS SP8 time-gated system. The STED depletion laser was co-aligned with the excitation laser and used to selectively deactivate the excited fluorophores surrounding the focal point, which allows an increased resolution of 30 to 40 nm by shrinking the point-spread function of the microscope. Images (1024 \times 1024 pixels) were acquired in both confocal and STED modes. Acquisition settings such as laser power, image size, pixel dwell times, line average, frame accumulation, and time-gating

interval (1- to 6-ns post-pulse time window) were optimized to achieve the best imaging quality. Deconvolution of STED images was performed using Huygens software (Scientific Volume Imaging) with the Huygens classical maximum likelihood estimation deconvolution algorithm.

Image processing and analysis

All images were exported from LAS X (Leica Microsystems) and further processed using Fiji software (National Institutes of Health). The brightness and contrast of all images were linearly adjusted across the entire image. To quantitatively analyze the diameter and distribution pattern of spectrin rings, lines across the structures were drawn and the intensity profiles were measured using Fiji or LAS X, and these were further analyzed using MATLAB (MathWorks Inc.). For diameter measurement, the raw intensity data from one single ring structure (characterized by twin peaks) were normalized, the positions of each peak were found, the corresponding x values were taken as boundaries of the ring structure, and the diameters of the ring structures were calculated. For distribution pattern analysis, a fast Fourier transform (FFT) algorithm was applied to the normalized intensity profiles, and the fundamental frequency was determined. To quantitatively analyze the disruption index of the spectrin rings in the hearing loss models, spectrin ring numbers were counted using Fiji software from each HC in the apical/middle/basal regions and normalized by the highest ring numbers from single HC at the corresponding region and developmental stage. The ring disruption index ranged from 0 to 1 (0 representing severe disruption and 1 representing no disruption). All the intensity, diameter, FFT, and ring disruption index data were plotted using GraphPad Prism (GraphPad Software Inc.), and all the figure layouts were prepared in Illustrator (Adobe Systems Inc.).

ABR audiometry

ABR is the method to assess hearing by measuring the hearing threshold. In this test, on the basis of Tucker-Davis Technology System III [Tucker-Davis Technologies (TDT), Gainesville, FL, USA], ABR was performed in a soundproof room and changes in the electrical activity of the brain in response to sound were recorded via electrodes that were placed on the scalp of the mouse (36). In detail, mice were placed on a 37°C heating pad in the sound-attenuated space to maintain their homeostasis after being anesthetized with ketamine (100 mg/kg) and xylazine (25 mg/kg). ABRs were recorded by using three needle electrodes placed over the vertex and bilaterally behind the pinnae. An MF1 magnetic speaker, a high-fidelity speaker for free-field presentation, was placed in front of the ear canal and used to generate sound. The ABR responses were elicited in tone bursts at five frequencies (4, 8, 16, 24, and 32 kHz). The acquired ABR response signal was amplified, averaged, and presented in a computer-based data acquisition system (BioSigRZ software, TDT, Gainesville, FL, USA). The sound pressure level for each frequency was performed between 15 and 90 dB (decibels SPL) in 5- or 10-dB steps. At each sound level, 1024 responses were averaged to get a reliable result. The ABR threshold was defined as the lowest SPL that could elicit a detectable response. All ABR tests were performed on mice older than P21.

VOR testing

Adult *Atoh1-sptbn1*^{-/-} and control mice (body weight, 20 to 25 g) were involved in the VOR testing experiments. A mouse was loaded on a horizontal turntable, with its head and body fixed in a specifically

developed holder. Miosis was conducted using 1% pilocarpine approximately 15 min before the test. In a dark environment, VOR was evoked by sinusoidal counter rotation (amplitude, $\pm 20^\circ$) that was performed horizontally by the turntable. The frequencies of the counter rotation were selected as 0.25, 0.5, and 1.0 Hz. The VOR response was recorded using two cameras (one for each eye) under the illumination of infrared light (940 nm) and, subsequently, analyzed using customized software based on eye-tracking algorithms and FFT.

Hearing damage model

For the noise-induced hearing damage model, awake adult mice in a wire mesh box were exposed to white noise (2 to 20 kHz) of 110 dB for 2 hours in a soundproof space. The white noise was generated and amplified in a TDT system and produced using four high-fidelity speakers placed above the box (37). After noise exposure, the mice were transferred to the standard animal facility for 1 day of recovery before the ABR test was performed. Immunofluorescence experiments of the cochlear specimens were then performed as described above.

Transmission electron microscopy

Cochlear specimens from P30 mice were fixed in 2.5% glutaraldehyde (in PBS, pH 7.2) at 4°C overnight. After dehydration in a graded series of ethanols, the specimens were embedded in araldite CY 212 (TAAB, Aldermaston, UK). Ultrathin sections were cut using a diamond knife in a direction parallel to the stereocilia and then stained with alcoholic uranyl acetate (Polysciences, Warrington, USA) and alkaline lead citrate (Sigma-Aldrich). After washing gently with distilled water, the sections were randomly examined with a JEM 1230 transmission electron microscope (JEOL Ltd., Tokyo, Japan).

Two-dimensional micromechanical model

A two-dimensional model of the cochlea was modified from a previous study (30). This model predicts the BM motion and the shearing motion between the tectorial membrane and the reticular lamina within an active organ of Corti in response to both acoustic and electrical excitations. The spectrin rings were introduced between the stereocilia bottom and the cuticular plate of the OHCs. The transverse BM motions were compared under the following conditions: normal spectrin rings, reduced spectrin rings, and no spectrin rings. The BM displacement was shown as $|W_{BM}|$ (nm). Normalized frequency was calculated as $\text{Freq}/\text{CF}(x_0)$, i.e., excitation frequencies were divided by the characteristic frequency at x_0 where the model geometry was taken from.

Quantification and statistical analysis

Statistical analyses were performed using Excel (Microsoft) and GraphPad Prism 6.0 software. Student's t test and one-way analysis of variance (ANOVA) were used to determine the statistical significance. $P < 0.05$ was considered significant. All replicate numbers (number of mice, number of spectrin rings, or number of OHCs and IHCs analyzed) are specifically indicated in the figure legends. When possible, all analyses were undertaken blind to genotype and/or development stage.

SUPPLEMENTARY MATERIALS

Supplementary material for this article is available at <http://advances.sciencemag.org/cgi/content/full/5/4/eaav7803/DC1>

Fig. S1. The spectrin structure in the cuticular plate of HCs.

Fig. S2. Localization and irregular distribution of FAM65B in *Atoh1-Sptbn1*^{-/-} mice.

Fig. S3. HC maintenance.

Fig. S4. Normal morphology and function of VHC in *Atoh1-Sptbn1*^{-/-} mice.
 Fig. S5. Spectrin rings are disrupted in OHCs of noise-induced hearing loss mice.
 Movie S1. Spectrin ring structure in cuticular plate of OHCs from an adult mouse.
 Movie S2. Spectrin structure in cuticular plate of VHCs from an adult mouse.

REFERENCES AND NOTES

- D. J. DeRosier, L. G. Tilney, The structure of the cuticular plate, an in vivo actin gel. *J. Cell Biol.* **109**, 2853–2867 (1989).
- L. G. Tilney, E. H. Egelman, D. J. DeRosier, J. C. Saunderson, Actin filaments, stereocilia, and hair cells of the bird cochlea. II. Packing of actin filaments in the stereocilia and in the cuticular plate and what happens to the organization when the stereocilia are bent. *J. Cell Biol.* **96**, 822–834 (1983).
- L. G. Tilney, D. J. DeRosier, Actin filaments, stereocilia, and hair cells of the bird cochlea: IV. How the actin filaments become organized in developing stereocilia and in the cuticular plate. *Dev. Biol.* **116**, 119–129 (1986).
- D. I. Scheffer, D.-S. Zhang, J. Shen, A. Indzhykulyan, K. D. Karaviti, Y. J. Xu, Q. Wang, J. J.-C. Lin, Z.-Y. Chen, D. P. Corey, XIRP2, an actin-binding protein essential for inner ear hair-cell stereocilia. *Cell Rep.* **10**, 1811–1818 (2015).
- F. Vranceanu, G. A. Perkins, M. Terada, R. L. Chidavaenzi, M. H. Ellisman, A. Lysakowski, Striated organelle, a cytoskeletal structure positioned to modulate hair-cell transduction. *Proc. Natl. Acad. Sci. U.S.A.* **109**, 4473–4478 (2012).
- D. N. Furness, S. Mahendrasingam, M. Ohashi, R. Fettiplace, C. M. Hackney, The dimensions and composition of stereociliary rootlets in mammalian cochlear hair cells: Comparison between high- and low-frequency cells and evidence for a connection to the lateral membrane. *J. Neurosci.* **28**, 6342–6353 (2008).
- L. G. Tilney, D. J. DeRosier, M. J. Mulroy, The organization of actin filaments in the stereocilia of cochlear hair cells. *J. Cell Biol.* **86**, 244–259 (1980).
- D. Drenckhahn, K. Engel, D. Höfer, C. Merte, L. Tilney, M. Tilney, Three different actin filament assemblies occur in every hair cell: Each contains a specific actin crosslinking protein. *J. Cell Biol.* **112**, 641–651 (1991).
- B. Kachar, A. Battaglia, J. Fex, Compartmentalized vesicular traffic around the hair cell cuticular plate. *Hear. Res.* **107**, 102–112 (1997).
- S.-i. Kitajiri, T. Sakamoto, I. A. Belyantseva, R. J. Goodyear, R. Stepanyan, I. Fujiwara, J. E. Bird, S. Riazuddin, S. Riazuddin, Z. M. Ahmed, J. E. Hinshaw, J. Sellers, J. R. Bartles, J. A. Hammer III, G. P. Richardson, A. J. Griffith, G. I. Frolenkov, T. B. Friedman, Actin-bundling protein TRIOBP forms resilient rootlets of hair cell stereocilia essential for hearing. *Cell* **141**, 786–798 (2010).
- V. Bennett, A. J. Baines, Spectrin and ankyrin-based pathways: Metazoan inventions for integrating cells into tissues. *Physiol. Rev.* **81**, 1353–1392 (2001).
- A. J. Baines, The spectrin-ankyrin-4-1-adducin membrane skeleton: Adapting eukaryotic cells to the demands of animal life. *Protoplasma* **244**, 99–131 (2010).
- M. N. Rasband, The axon initial segment and the maintenance of neuronal polarity. *Nat. Rev. Neurosci.* **11**, 552–562 (2010).
- M. Krieg, A. R. Dunn, M. B. Goodman, Mechanical control of the sense of touch by β -spectrin. *Nat. Cell Biol.* **16**, 224–233 (2014).
- V. Bennett, J. Davis, W. E. Fowler, Brain spectrin, a membrane-associated protein related in structure and function to erythrocyte spectrin. *Nature* **299**, 126–131 (1982).
- K. Xu, G. Zhong, X. Zhuang, Actin, spectrin, and associated proteins form a periodic cytoskeletal structure in axons. *Science* **339**, 452–456 (2013).
- G. Zhong, J. He, R. Zhou, D. Lorenzo, H. P. Babcock, V. Bennett, X. Zhuang, Developmental mechanism of the periodic membrane skeleton in axons. *eLife* **3**, e04581 (2014).
- E. D'Este, D. Kamin, F. Göttfert, A. el-Hady, S. W. Hell, STED nanoscopy reveals the ubiquity of subcortical cytoskeleton periodicity in living neurons. *Cell Rep.* **10**, 1246–1251 (2015).
- K. Legendre, S. Safieddine, P. Küssel-Andermann, C. Petit, A. El-Amraoui, II- β V spectrin bridges the plasma membrane and cortical lattice in the lateral wall of the auditory outer hair cells. *J. Cell Sci.* **121**, 3347–3356 (2008).
- M. Cortese, S. Papal, F. Pisciotto, A. B. Elgoyhen, J.-P. Hardelin, C. Petit, L. F. Franchini, A. El-Amraoui, Spectrin β V adaptive mutations and changes in subcellular location correlate with emergence of hair cell electromotility in mammals. *Proc. Natl. Acad. Sci. U.S.A.* **114**, 2054–2059 (2017).
- S. T. Hess, T. P. K. Girirajan, M. D. Mason, Ultra-high resolution imaging by fluorescence photoactivation localization microscopy. *Biophys. J.* **91**, 4258–4272 (2006).
- E. Betzig, G. H. Patterson, R. Sougrat, O. W. Lindwasser, S. Olenych, J. S. Bonifacino, M. W. Davidson, J. Lippincott-Schwartz, H. F. Hess, Imaging intracellular fluorescent proteins at nanometer resolution. *Science* **313**, 1642–1645 (2006).
- M. J. Rust, M. Bates, X. Zhuang, Sub-diffraction-limit imaging by stochastic optical reconstruction microscopy (STORM). *Nat. Methods* **3**, 793–796 (2006).
- B. Huang, S. A. Jones, B. Brandenburg, X. Zhuang, Whole-cell 3D STORM reveals interactions between cellular structures with nanometer-scale resolution. *Nat. Methods* **5**, 1047–1052 (2008).
- M. Rief, J. Pascual, M. Saraste, H. E. Gaub, Single molecule force spectroscopy of spectrin repeats: Low unfolding forces in helix bundles. *J. Mol. Biol.* **286**, 553–561 (1999).
- J. C. Lee, D. E. Discher, Deformation-enhanced fluctuations in the red cell skeleton with theoretical relations to elasticity, connectivity, and spectrin unfolding. *Biophys. J.* **81**, 3178–3192 (2001).
- J. He, R. Zhou, Z. Wu, M. A. Carrasco, P. T. Kurshan, J. E. Farley, D. J. Simon, G. Wang, B. Han, J. Hao, E. Heller, M. R. Freeman, K. Shen, T. Maniatis, M. Tessier-Lavigne, X. Zhuang, Prevalent presence of periodic actin-spectrin-based membrane skeleton in a broad range of neuronal cell types and animal species. *Proc. Natl. Acad. Sci. U.S.A.* **113**, 6029–6034 (2016).
- B. Zhao, Z. Wu, U. Müller, Murine Fam65b forms ring-like structures at the base of stereocilia critical for mechanosensory hair cell function. *eLife* **5**, e14222 (2016).
- S. Safieddine, A. El-Amraoui, C. Petit, The auditory hair cell ribbon synapse: From assembly to function. *Annu. Rev. Neurosci.* **35**, 509–528 (2012).
- G. Ni, S. J. Elliott, J. Baumgart, Finite-element model of the active organ of Corti. *J. R. Soc. Interface* **13**, 20150913 (2016).
- D. H. Smith, J. A. Wolf, T. A. Lusardi, V. M.-Y. Lee, D. F. Meaney, High tolerance and delayed elastic response of cultured axons to dynamic stretch injury. *J. Neurosci.* **19**, 4263–4269 (1999).
- L. Luo, D. D. M. O'Leary, Axon retraction and degeneration in development and disease. *Annu. Rev. Neurosci.* **28**, 127–156 (2005).
- Y. Ikeda, K. A. Dick, M. R. Weatherspoon, D. Gincel, K. R. Armbrust, J. C. Dalton, G. Stevanin, A. Dürr, C. Zühlke, K. Bürk, H. B. Clark, A. Brice, J. D. Rothstein, L. J. Schut, J. W. Day, L. P. W. Ranum, Spectrin mutations cause spinocerebellar ataxia type 5. *Nat. Genet.* **38**, 184–190 (2006).
- C.-C. Wang, X. R. Ortiz-Gonzalez, S. W. Yum, S. M. Gill, A. White, E. Kelter, L. H. Seaver, S. Lee, G. Wiley, P. M. Gaffney, K. J. Wierenga, M. N. Rasband, β IV spectrinopathies cause profound intellectual disability, congenital hypotonia, and motor axonal neuropathy. *Am. J. Hum. Genet.* **102**, 1158–1168 (2018).
- H. Yang, X. Xie, M. Deng, X. Chen, L. Gan, Generation and characterization of *Atoh1-Cre* knock-in mouse line. *Genesis* **48**, 407–413 (2010).
- J. Wang, T. Menchenon, S. Yin, Z. Yu, M. Bance, D. P. Morris, C. S. Moore, R. G. Korneluk, G. S. Robertson, Over-expression of X-linked inhibitor of apoptosis protein slows presbycusis in C57BL/6J mice. *Neurobiol. Aging* **31**, 1238–1249 (2010).
- L. Liu, Y. Chen, J. Qi, Y. Zhang, Y. He, W. Ni, W. Li, S. Zhang, S. Sun, M. M. Taketo, L. Wang, R. Chai, H. Li, Wnt activation protects against neomycin-induced hair cell damage in the mouse cochlea. *Cell Death Dis.* **7**, e2136 (2016).

Acknowledgments: We thank the Shanghai Municipal Government and ShanghaiTech University for financial support, J. Gao (Shandong University) for providing *Atoh1-Cre* mice, and the Bioimaging Core Facilities of the iHuman Institute and the animal facility of National Center for Protein Science Shanghai for their support. We also thank K. Zhang, J. Wang, Y. Li, F. Hao, and H. Liu for helpful discussions. **Funding:** This work was supported by the Strategic Priority Research Program of the Chinese Academy of Sciences (XDA16010303), the National Key Research and Development Program of China (2016YFC0905900 to G.Z. and 2017YFC1001300 to G.Z. and S.H.), the National Natural Science Foundation of China (31771130 to G.Z.), the National Key Research and Development Program of China (2015CB965000 and 2017YFA0103900 to R.C.), the 2015 Thousand Youth Talents Plan of China (to G.Z. and R.C.), the National Natural Science Foundation of China (31200743 to Y.L., 31671063 to S.H., and 81622013, 81470692, and 31500852 to R.C.), Boehringer Ingelheim Pharma GmbH, and the Huo Yingdong Education Foundation. **Author contributions:** G.Z., R.C., S.H., and M.T. conceived and designed the experiments. Y.L., J.Q., and X.C. performed most of the experiments and data analyses. Y.L., J.Q., C.C., H.L., and C.T. acquired the super-resolution fluorescence image data. J.Q. and W.Z. acquired the ABR data. J.Q. acquired the electron microscopy data. G.Z., Y.L., J.Q., C.C., H.L., X.C., G.N., Y.Z., and C.T. contributed to data analysis. G.Y., M.T., and C.Z. discussed data analysis, interpretation, and presentation. G.Z., Y.L., and J.Q. wrote the manuscript with contributions from all authors. **Competing interests:** The authors declare that they have no competing interests. **Data and materials availability:** All data needed to evaluate the conclusions in the paper are present in the paper and/or the Supplementary Materials. Additional data related to this paper may be requested from the authors.

Submitted 18 October 2018
 Accepted 1 March 2019
 Published 17 April 2019
 10.1126/sciadv.aav7803

Citation: Y. Liu, J. Qi, X. Chen, M. Tang, C. Chu, W. Zhu, H. Li, C. Tian, G. Yang, C. Zhong, Y. Zhang, G. Ni, S. He, R. Chai, G. Zhong, Critical role of spectrin in hearing development and deafness. *Sci. Adv.* **5**, eaav7803 (2019).